Measurement Science and Technology

A modified moiré technique for three-dimensional surface topography

Meas. Sci. Technol. **13** (2002) 613–622 PII: S0957-0233(02)28979-1

A modified moiré technique for three-dimensional surface topography

L D'Acquisto[1], L Fratini[2] and A M Siddiolo[1]

[1] Dipartimento di Meccanica ed Aeronautica, University of Palermo, viale delle Scienze, 90128 Palermo, Italy
[2] Dipartimento di Tecnologia e Produzione Meccanica, University of Palermo, viale delle Scienze, 90128 Palermo, Italy

E-mail: dacquisto@dima.unipa.it and abaqus@dtpm.unipa.it (L Fratini)

Received 13 September 2001, in final form 29 January 2002, accepted for publication 22 February 2002
Published 19 March 2002
Online at stacks.iop.org/MST/13/613

Abstract
In this paper we present an optical technique based on the shadow moiré method which allows the measurement and digitization of three-dimensional surfaces. The technique was tested through experimental work and the results were compared with those obtained by a coordinate measuring machine. Moving from the conventional shadow moiré method, new features were implemented enabling us to overcome the main shortcomings of the conventional moiré method. These include the need to assign the fringe order, the incapability of discerning concavity or convexity, the poor resolution and the complexity in the signal processing. All these problems have been solved by adding an element to generate a carrier fringe pattern to the equipment of the conventional shadow moiré technique and processing the obtained signal using the Fourier transform method. The proposed technique was applied to obtain external surfaces of sheet metal stamped parts. The experimental results show the effectiveness of this technique.

Keywords: three-dimensional surface measurement, shadow moiré topography, reverse engineering

1. Introduction

A number of techniques are currently suitable for measuring three-dimensional (3D) object surfaces. These are based on both contact and non-contact procedures and present different sensitivities. However, they require very complex set-ups, which are troublesome to implement within an industrial environment. In such techniques, the coordinate measuring machine (CMM) is widely utilized; this equipment is very effective but it is time consuming, since it performs single-point measurements, thus requiring a great number of points to describe completely a surface with a low level of uncertainty.

The aim of the present work is to set up an automated user-friendly technique, using common equipment which gives adequate accuracy to resolve out-of-plane elevations of some micrometres over a depth range of a few millimetres. This is the case of shape defect insurgence in fully 3D stamped sheets of limited dimensions characterized by steep surfaces.

After an accurate review of the techniques illustrated in the literature [1, 2], a choice was made to use out-of-plane displacement moiré techniques [3–6].

The out-of-plane displacement can be independently measured by shadow moiré or by projection moiré [6]. Shadow moiré uses the reference gratings superimposed on its shadow to form a moiré pattern. Projection moiré can be divided into three categories according to its optical arrangement: one projector, deformation moiré [7]; one projector, topography moiré [8–10]; and two projector moiré [11]. The first method uses double exposure to superimpose the original grating onto a deformated grating to generate a moiré pattern. The second method projects one grating onto the specimen and this is viewed through another grating. The third method produces the moiré fringes by two projected gratings. Shadow moiré presents the disadvantage that the master grating has a similar size to the measured object. Projection moiré has the advantage over shadow moiré that no element of the apparatus

0957-0233/02/040613+10$30.00

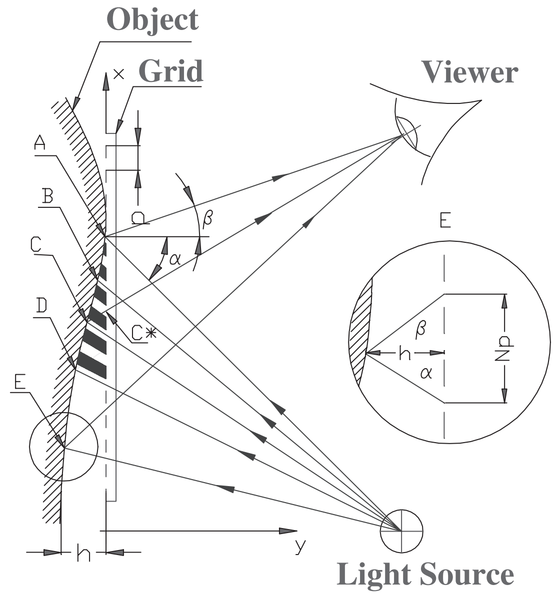

Figure 1. Classical shadow moiré set-up.

is required to be close to the measured object. It has the disadvantage that the optical systems are more complicated and the individual lines of the projected gratings must be resolved in the observation leg. To cope with the above requirements, shadow moiré has been chosen as the measuring method because the configuration is simple, robust and it requires only a single image to obtain a 3D measurement.

The proposed technique combines shadow moiré and Fourier transform (FT) profilometry [12–14], introducing a carrier fringe pattern to obtain a phase modulated signal with high spatial frequency, fit for the use of the FT method. It shows some advantages in terms of procedure automation and signal processing, compared to fringe shifting and phase stepping shadow moiré techniques [15–22].

In the literature, several researchers have proposed techniques to increase the accuracy and the resolution of contouring methods [20–23], mainly based on the phase shifting shadow moiré method. In the proposed technique a spatial carrier pattern, generated by sloping the moiré grid, is directly observed on an auxiliary reference block, which is introduced in the experimental set-up. The simultaneous measurement of the instantaneous carrier fringe pattern and of the modulated pattern on the object surface enables us to avoid the use of a precise mechanical rotation stage for the grid positioning and of a precise mechanical translation stage for the object itself. Therefore the technique requires only a single moiré pattern, i.e. one phase distribution is acquired, to obtain the object height distribution. The required geometrical resolution is obtained by designing a particular set-up which is able to provide an optical full field signal, suitable for processing with the FT method. This technique has been applied to obtain external surfaces of sheet metal stamped parts, namely rectangular boxes.

In the following sections the proposed technique is presented, highlighting the main features both of the utilized set-up and of the *ad hoc* computing procedure developed by the authors.

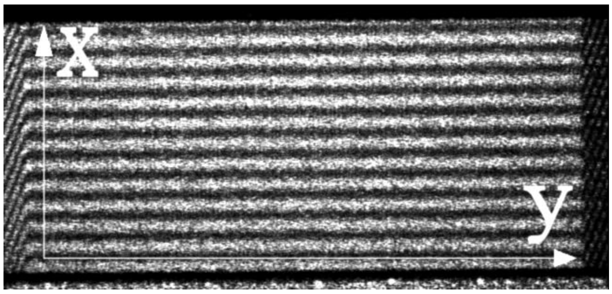

Figure 2. Carrier fringe pattern.

2. The experimental set-up

According to figure 1, the shadow moiré pattern represents on the surface under investigation the loci of points of constant out-of-plane elevation.

Fringe patterns generated by moiré techniques generally show a low fringe frequency, not adequate for the application of the FT method [17, 24–27]. This is due to the fact that the surfaces under investigation are usually nearly plane and to the poor depth of field that in practice puts limits on the surfaces that can be investigated by these techniques. A perfectly flat surface positioned parallel to the grid plane would show no fringes at all. Under such circumstances a small grid slope determines a carrier signal characterized by a fringe pattern with parallel evenly spaced fringes. Furthermore the use of incoherent light does not allow fringe generation when the grid sloping angle exceeds a few degrees; in turn the use of a coherent laser source permits us to obtain a carrier pattern with an adequate spatial frequency, as shown in figure 2. Exact information on the carrier pattern is obtained by placing a reference steel block, with sharp shape and dimensions, next to the specimen whose surfaces have to be acquired; the exact geometrical definition of the reference block is also useful to calibrate the geometrical scale in the acquired image. In this way the carrier pattern will be generated on the front surface of the reference block. This pattern, properly named *carrier pattern*, is described by the expression

$$i_c(x, y) = i_{c0}(x, y) + i_{c1}\cos(\omega_c x + \varphi_c) + i_{cn}(x, y) \quad (1)$$

where $i_{c0}(x, y)$ is the intensity bias, $i_{c1}(x, y)$ is the intensity modulation of the carrier signal, and $i_{cn}(x, y)$ is the intensity of the high frequency additive noise. x is the axis normal to the fringe direction, and φ_c is the value of the initial phase, that can be set equal to zero without any loss in information. ω_c is defined as

$$\omega_c = \frac{2\pi n_f}{l}\left[\frac{\text{rad}}{\text{mm}}\right] \quad (2)$$

where n_f is the number of fringes measured along the x-direction over a segment of length l.

The original signal, associated with the shape of the surface to measure, is then utilized to phase modulate the carrier signal in figure 2, obtaining the modulated signal $i_m(x, y)$, which is shown in figure 3, expressed by

$$i_m(x, y) = i_{m0}(x, y) + i_{m1}(x, y) \times \cos[\omega_c x + \varphi_c + \varphi(x, y)] + i_{mn}(x, y) \quad (3)$$

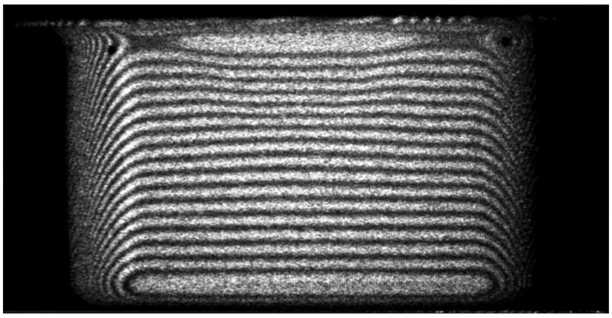

Figure 3. Modulated fringe pattern.

with notations 0, 1 and n having the same meanings as in equation (1). The term $\varphi(x, y)$ contains the information about the topography of the object surface.

The utilized experimental set-up, shown in figures 4(*a*) and (*b*), consists of the following items:

- a 35 mW He–Ne laser light source;
- a moiré grid on a glass plate (Graticules mod. SAG4) with rectilinear parallel fringes with pitch $p = 0.127$ mm;
- a prismatic block to hold the specimen (painted white matt to visualize the carrier optical signal on the front surface);
- a CCD B/W digital camera (SVS-Vistek CA085A10) (1280 × 1024 pixel);
- a camera lens Nikkor AF Micro 70–210 mm, 1:4 D;
- a Pentium III class PC.

3. Signal processing

As reported in the previous section, the full field data on the out-of-plane elevations $h'(x, y)$ to be measured are related to the $\varphi(x, y)$ term in equation (3). Computing a FT of $I_m(x, y)$, after a proper choice of the frequency of the carrier signal, i.e. proper inclination of the moiré grid, a frequency spectrum $I_m(\omega)$ is obtained of the modulated signal i_m where the side bands of the low-frequency background signal and of the high-frequency additive noise are separated from the frequency band of the signal of interest, as is illustrated in figure 5.

Under these conditions the average component of the signal and the high-frequency noise content can be effectively removed, obtaining

$$\psi(x, y) = \omega_c x + \varphi(x, y) \tag{4}$$

which carries the measurement information.

At each point $\psi(x, y)$ is proportional to the distance $h'(x, y)$ of the object surface from the moiré grid in its sloped position; such a function is, at a different scale, the full field information about the fringe order $N(x, y)$. The spatial frequency ω_c is independently obtained from the carrier pattern visualized on the front surface of the reference steel block (see figure 4(*a*)).

3.1. Fourier transform method

Since a column-ordered data processing has been developed, for reason of simplicity, in the following section only the direction normal to the fringes (i.e. parallel to the x-axis) is taken into account, so that only processing of one column is described.

Light intensity along the x-direction, according to the notation utilized in equation (3), is rewritten as

$$i_m(x) = i_0(x) + i_1(x)\cos[\psi(x)] + i_n(x). \tag{5}$$

Removing the i_0 and i_n terms, under the above assumptions, the *in-phase* signal i_p will be

$$i_p(x) = i_1(x)\cos[\psi(x)]. \tag{6}$$

In fact, no exact information on the local amplitude of the light intensity i_1 is available to obtain directly the phase information $\psi(x)$. It is worth noting that $\psi(x)$ could be easily calculated, removing the influence of the local value of the light intensity $i_1(x)$, from the expression

$$\psi(x) = \arctan\left[\frac{i_q(x)}{i_p(x)}\right] = \arctan\left\{\frac{i_1(x)\sin[\psi(x)]}{i_1(x)\cos[\psi(x)]}\right\} \tag{7}$$

if the in-quadrature signal i_q were known, where

$$i_q(x) = i_1(x)\sin[\psi(x)]. \tag{8}$$

The information related to $\psi(x)$ would be obtained as a periodic function, defined in the range $[-\pi/2, \pi/2]$. The variation range of $\psi(x)$ usually exceeds the mentioned range. Therefore the discontinuous phase $\psi'(x)$ is obtained from equation (7). Applying an unwrapping procedure to $\psi'(x)$, the continuous phase $\psi(x)$ can be extracted as

$$\psi(x) = \psi'(x) \pm k\pi \tag{9}$$

by incrementing or decrementing the k index according to the modulo π jump in the $\psi'(x)$ value.

3.2. Procedure steps

Fringe pattern analysis with the FT method enables the discontinuous phase along profiles and surfaces to be obtained in a semi-automated way, requiring just few indications by the operator.

Moving from equations (5) and (6), the expression of the light intensity can be rewritten in the form

$$\begin{aligned} i_m &= i_0 + i_p + i_n = i_0 + \tfrac{1}{2}i_1[(\cos\psi + \mathrm{j}\sin\psi) \\ &\quad + (\cos\psi - \mathrm{j}\sin\psi)] + i_n = i_0 + i + \bar{i} + i_n \end{aligned} \tag{10}$$

where

$$i = \tfrac{1}{2}i_1(\cos\psi + \mathrm{j}\sin\psi) = \tfrac{1}{2}i_1\mathrm{e}^{\mathrm{j}\psi} \tag{11}$$

according to Euler's formula. In equation (10) the overbar denotes the conjugated complex number. In equation (11) the complex number is expressed utilizing both the Cartesian and the polar notation; the real and the imaginary parts are respectively coincident with the in-phase signal (6) and with the in-quadrature signal (8). The aim of the method is to obtain these parameters through proper transformations in the frequency domain, in order to evaluate the phase signal $\psi(x, y)$ from equation (7).

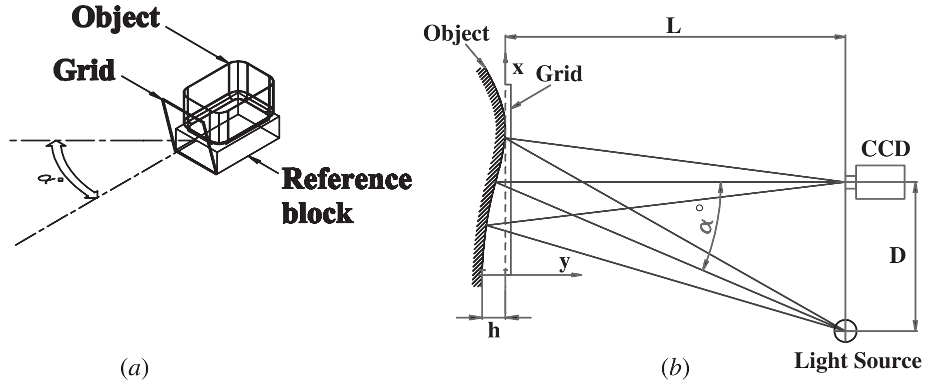

Figure 4. Proposed experimental set-up.

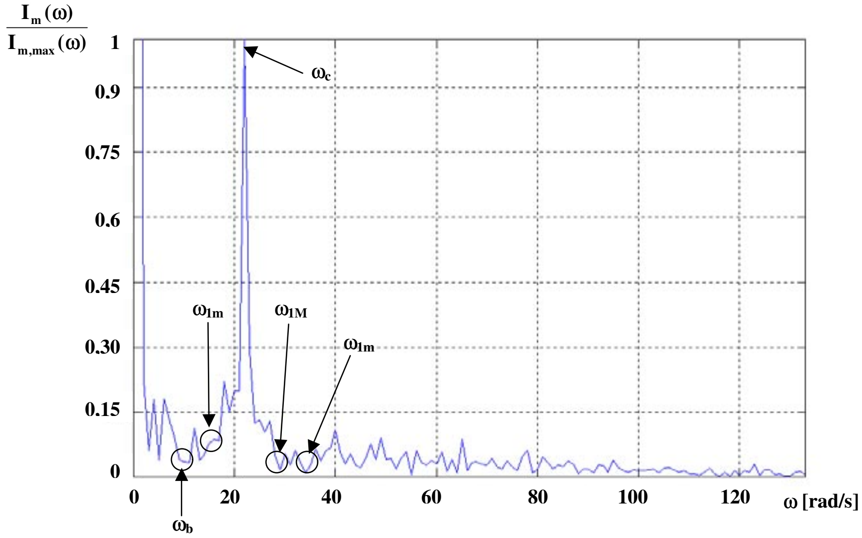

Figure 5. Obtained signal spectrum.
(This figure is in colour only in the electronic version)

The main steps of the method can be summarized as follows.

3.2.1. FT evaluation of the acquired signal. On the basis of the well-known linearity properties of FT, it can be written

$$F[i_m] = I_m(\omega) = I_0(\omega) + I(\omega-\omega_c) + \bar{I}(\omega+\omega_c) + I_n(\omega). \quad (12)$$

3.2.2. FT evaluation of the in-phase signal. Since i_0, i_1 and $\varphi(x, y)$ often vary rather slowly with respect to the carrier signal, their spectral contents will lie apart from the carrier frequency ω_c, as shown in figure 5. In this way, $I_0(\omega)$ and $I_n(\omega)$ can be easily removed multiplying $I_m(\omega)$ (12) by a proper band-pass filter function $\Phi(\omega)$ [28], whose characteristics have to be selected by the operator. The choice of the bandwidth limits, aiming to preserve the spectrum content among ω_{1m} and ω_{1M}, results immediately by the observation of the signal spectrum in figure 5. This operation determines no losses of information in the core signal and in turn it removes from $I_m(\omega)$ those terms corresponding to ineffective phenomena such as the non-uniform reflectivity of the object surfaces and the high-frequency noise (electronic noise etc). The level of intervention of the operator is then limited and elementary; this makes the method semi-automatic.

In this way, the filtering operation gives an approximated FT of the *in-phase* signal (6) in the form

$$F[i_p] = I_p(\omega) = I(\omega - \omega_c) + \bar{I}(\omega + \omega_c) \cong I'_p(\omega)$$
$$= I_m(\omega)\Phi(\omega). \quad (13)$$

Here $\Phi(\omega)$ is a *rect* function of width $(b - a)$, centred at $(b - a)/2$, where a and b respectively are the lower and upper bandwidth limits of the filter $\Phi(\omega)$.

The term $I'_p(\omega)$ (13) is an approximation of the FT of the *in-phase* signal since $F[i(x)] = I(\omega - \omega_c)$ can have non-zero terms outside the range $[a, b]$, which can be neglected in the proposed application.

3.2.3. FT evaluation of the in-quadrature signal. To obtain $\psi(x)$, as shown in equation (7), the in-quadrature signal i_q is necessary. In the literature, two different methods have been reported [12, 25–27] which have been demonstrated to lead to the same results [29]. They provide an analytical signal $i_a(x)$, whose real part is the *in-phase* signal of interest and the imaginary part is the wanted *in-quadrature* signal. In [29], by the use of the Hilbert transform, the analytical signal has been obtained as expressed by the transformation

$$I_a(\omega) = 2U(\omega)I'_p(\omega) \cong 2I(\omega - \omega_c) \qquad (14)$$

where $U(\omega)$ is the classical unit step function. In this way, having $I'_p(\omega)$ (13), which is the best available approximation of the FT *in-phase* signal, the Hilbert transform [27, 29] was therefore applied, giving an analytical signal $I_a(\omega)$ as a result.

Once the inverse FT of $I_a(\omega)$ is calculated, the complex signal $i_a(x)$ can be obtained as

$$i_a(x) = F^{-1}[I_a(\omega)] \cong 2i(x) = i_1(\cos\psi + \mathrm{j}\sin\psi). \qquad (15)$$

3.2.4. Evaluation of the discontinuous phase. The discontinuous phase of the signal, denoted by $\psi'(x)$, is simply obtained as

$$\psi'(x) = \arctan\left\{\frac{\mathrm{Im}\,[i_a(x)]}{\mathrm{Re}\,[i_a(x)]}\right\} \cong \arctan\left[\frac{i_q(x)}{i_p(x)}\right]. \qquad (16)$$

It should be observed that the phase information associated with $I'_p(\omega)$ is a monotonic increasing function, since it is related to the point-by-point distance between the moiré grid and the object surface, due to the frequency modulation operated when the carrier frequency is introduced (i.e. sloping the moiré grid). Hence, applying the unwrapping algorithm to the $\psi'(x)$ signal gives the continuous phase function $\psi(x)$. Such a procedure is repeated column-wise to get the overall phase signal in the x, y domain. Then, with

$$\psi(x, y) = \varphi(x, y) + \omega_c x \qquad (17)$$

it is possible to obtain the desired signal $\varphi = \varphi(x, y)$ from the above equation by subtracting the experimentally known quantity $\omega_c x$ from the function $\psi'(x, y)$. The carrier frequency value ω_c is separately measured from the acquired image of the fringe pattern displayed on the front surface of the prismatic block, used as reference (figure 2).

The proposed technique therefore enables continuous phase information to be obtained over the whole fringe pattern of interest, in a semi-automated way, by simultaneously performing the operation of centre fringe localization, fringe order numbering and overcoming the well-known limit of discerning concavity and convexity.

3.2.5. Phase-to-height conversion. With reference to figure 1, the known relation between the phase value φ and the distance of the observed point from the moiré grid, once the carrier signal has been removed (i.e. the grid is supposed to be vertical), is expressed as

$$h = \frac{pN}{\tan\alpha + \tan\beta}. \qquad (18)$$

With $N = \varphi(x, y)/2\pi$, where α and β are as represented in figure 1, equation (18) becomes

$$h = \frac{p\varphi(x, y)}{2\pi(\tan\alpha + \tan\beta)}. \qquad (19)$$

The capability of the method for full field resolution of fractional fringe orders comes out clearly, with a substantial improvement in measurement resolution compared to the classical shadow moiré method, by processing just one image for each object surface.

Equation (19) can be utilized if the vision angle β and the lighting angle α (see figure 4(*b*)) do not vary over the entire object surface. To satisfy this condition, the geometrical characteristics L and D of the experimental set-up (L denotes the working distance and D the distance between the CCD camera and the light source as shown again in figure 4(*b*)) were chosen according to the expression

$$\tan\alpha + \tan\beta = \frac{D}{L}. \qquad (20)$$

Otherwise, setting $L/D \gg 1$ to be the condition of an infinite point of view can be assumed.

4. Maximum range of measurement

The choice of the carrier frequency w_c value should allow us to bring the frequency content $I_p(\omega)$ to a frequency range apart from those of $I_0(\omega)$ and $I_n(\omega)$, in order to effectively apply the FT method. This condition can be observed in figure 5.

This constraint can be expressed by a relation containing the value of the carrier frequency, a few geometrical parameters of the experimental set-up indicated in figure 4(*b*) (namely D and L) and a parameter depending on the geometry of the surface to measure.

With reference to the spectrum of the acquired signal, where w_b denotes the highest frequency of the average component $I_0(\omega)$, w_{1m} denotes the lowest frequency of the *in phase* signal $I_p(\omega)$, w_{1M} denotes the highest frequency of the *in phase* signal $I_f(\omega)$ and w_{nm} denotes the lowest frequency of the noise signal $I_n(\omega)$, for an effective filtering action [28] the following conditions have to be verified:

$$\begin{aligned} \omega_{1M} &< \omega_{nm} \\ \omega_b &< \omega_{1m}. \end{aligned} \qquad (21)$$

After some algebra (see the appendix) the requested filtering conditions result in the inequality

$$\left|\frac{\partial h}{\partial x}\right|_M < \frac{1}{3} f_c \frac{Lp}{D}. \qquad (22)$$

5. Evaluation of uncertainty

The relation between the distance $h(x, y)$ of the generic point in the object surface from the reference grid (when in the vertical position) and the value of the argument $\varphi(x, y)$ of the circular function is

$$h(\psi, p, \alpha, \beta) = \frac{N(x, y)p}{\tan\alpha + \tan\beta} = \frac{\psi(x, y)p}{2\pi(\tan\alpha + \tan\beta)} \qquad (23)$$

where $\psi(x, y)$ is the argument value of the circular function, evaluated with the procedure described above, and p is the moiré grid pitch. α is the angle between the direction of the light source and the normal to the vertical surface of the reference block, and β is the angle between the CCD axis and again the normal to the vertical surface of the reference block.

With reference to input-independent variables, in order to evaluate the combined uncertainty $u_c(h)$ [30] on the parameter $h(x, y)$, contributions from the following elements must be taken into account:

(a) pitch p of the moiré grid;
(b) measurement of the unwrapped phase $\psi(x, y)$ (the value of the discontinuous phase, which is effectively acquired, has to be considered);
(c) measurement of the angle α;
(d) measurement of the angle β;
(e) uncertainty introduced by the geometric interpolation due to the different $x \times y$ dimensions of the CCD sensor and of the array of the A/D conversion board;
(f) uncertainty introduced by the A/D conversion;
(g) uncertainty due to the electronic noise.

In the developed application the uncertainty sources (a)–(d) have been taken into account, since they were found to be significant, while (e)–(g) were negligible. In particular:

(e) such a source is not relevant since the matrix dimensions of both the CCD sensor and the A/D conversion board were very similar, so that mismatch was negligible;
(f) the contribution to uncertainty related to the A/D signal conversion, given the linear variability of the phase information within a period of the sine function, depends on the minimum number of pixels utilized to digitize the highest frequency sinusoidal component of the measurement signal—the spatial sampling frequency utilized to acquire the images was about 60 pixels mm^{-1};
(g) given both the stationary properties of the measurements, the long acquisition time interval and the high S/N ratio of the CCD camera utilized, the contribution to uncertainty due to the electronic noise was neglected—this assumption was thoroughly confirmed by the analysis performed over several different images.

On the basis of equation (23), relating the dependent variable h to the parameters ψ, p, α and β, the sensitivity coefficients to be utilized in the uncertainty evaluation have been obtained as

$$\frac{\partial h}{\partial \psi} = \frac{p}{2\pi(\tan\alpha + \tan\beta)} \tag{24a}$$

$$\frac{\partial h}{\partial p} = \frac{\psi(x, y)}{2\pi(\tan\alpha + \tan\beta)} \tag{24b}$$

$$\frac{\partial h}{\partial \alpha} = -\frac{\psi(x, y)p}{2\pi(\tan\alpha + \tan\beta)^2\cos^2\alpha} \tag{24c}$$

$$\frac{\partial h}{\partial \beta} = -\frac{\psi(x, y)p}{2\pi(\tan\alpha + \tan\beta)^2\cos^2\beta}. \tag{24d}$$

The standard uncertainty values to calculate the combined uncertainty are reported below.

The evaluation of the standard uncertainty $u(\psi)$ has to be developed through experiments. In figure 2 the fringe field of the carrier signal is shown; as already mentioned, it can be approximated by a sinusoidal function as

$$i_c(x, y) = i_c \cos[\psi(x)]. \tag{25}$$

The surface on which the fringe pattern occurs is sharply flat and therefore it was used as a measurement reference. In order to evaluate the discrepancies between the $m \times n$ performed measurement (where m and n are the dimensions of the acquired image matrix) and the surface of the reference plate, local values of phase ψ were obtained by the analysis of both the experimental fringe pattern and the theoretical field generated on a perfectly flat surface. The frequency distribution of the obtained error is reported in figure 6; it is important to observe that the error distribution is unimodal with an average value close to zero. Assuming a normal distribution, the standard uncertainty was then calculated as the standard deviation of the distribution itself, obtaining

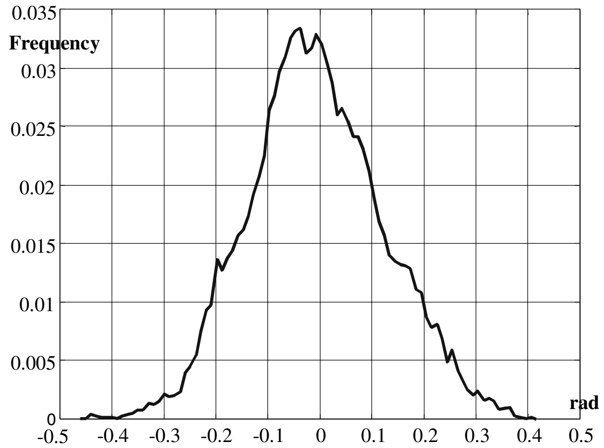

Figure 6. Phase error distribution.

$$\sigma = 0.1310 \text{ rad} = u(\psi) = 0.1310 \text{ rad}. \tag{26}$$

The resolution of the Zeiss Jena microscope, used to measure the moiré grid pitch, was found to be equal to 0.0005 mm. Having no uncertainty data provided by the manufacturer, a rectangular distribution was assumed. The calculated standard uncertainty is then

$$u(p) = 0.68 \times 0.0005 = 0.000\,34 \text{ mm}. \tag{27}$$

The estimated error limit on the setting of both the vision angle (β) and the lighting angle (α) (figure 1) is 0.5°. Again, for these two parameters a rectangular distribution is assumed. In this way, the calculated standard uncertainty is

$$u(\alpha) = u(\beta) = \frac{2}{3}0.5\frac{\pi}{180} \text{ rad} = 0.0059 \text{ rad}. \tag{28}$$

The above reported standard uncertainty values for the influence quantities taken into account, which are assumed to be independent, allow the combined standard uncertainty $u_c(h)$ to be evaluated utilizing the known expression

$$u_c(h) = \sqrt{\sum_{i=1}^{4}\left(\frac{\partial h}{\partial x_i}\right)^2 u(x_i)^2} = 0.0107 \text{ mm}. \tag{29}$$

The proposed measurement technique allows maximum levels of combined standard uncertainty $u_c(h)$ of about 10 μm to be obtained. Assuming a coverage factor $k = 2$, the extended uncertainty is then equal to

$$U = ku_c(h) = 21.4\ \mu\text{m}. \tag{30}$$

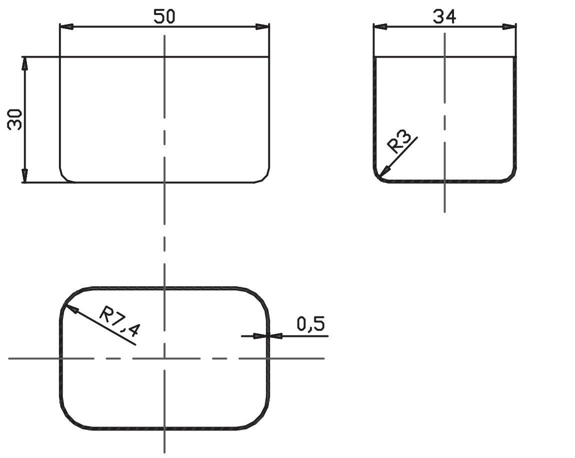

Figure 7. Specimen design (all the dimensions are in millimetres).

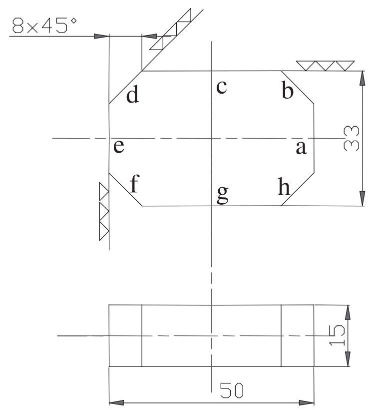

Figure 8. Reference block design (all the dimensions are in millimetres).

6. Application

The proposed measurement technique was applied to the evaluation of the whole lateral surface of a deep drawn steel component, whose geometry and nominal dimensions are reported in figure 7. The peculiar lateral contour of the considered specimen was acquired in eight different images.

A procedure aimed at assembling the different object surfaces was set up in order to obtain the complete lateral surface of the fully 3D stamped part. With this purpose an octagonal section reference block was manufactured (figure 8) with the aim both to allow a sharp determination of the carrier signal and to evaluate the rotation angle needed to assemble the eight single object surfaces to obtain the original whole specimen lateral surface. A typical fringe pattern field is reported in figure 9, including also the carrier fringe pattern, visualized on the reference block.

In the subsequent image acquisition of each portion of the lateral contour of the investigated stamped part, the relative rotation angle of each portion was exactly determined, getting rid of the overlapping areas. It should be observed that each single acquired portion presents limited overlapping areas with the two contiguous images.

Basically, in the rebuilding procedure, a preliminary rigid translation of the images was operated by utilizing proper markers placed on the surfaces themselves. Then, one surface was fixed in the space and the subsequent surface was stepwise rotated. The procedure was iterated, by the use of a least-squares fit technique [31], until a perfect fit of each couple of contiguous overlapped areas was obtained. In other words, assuming the reference system of the first image as the global one, all other local reference systems were roto-translated to coincide with the global one.

The eight images acquired for the evaluation of the total lateral surface of the drawn part are reported in

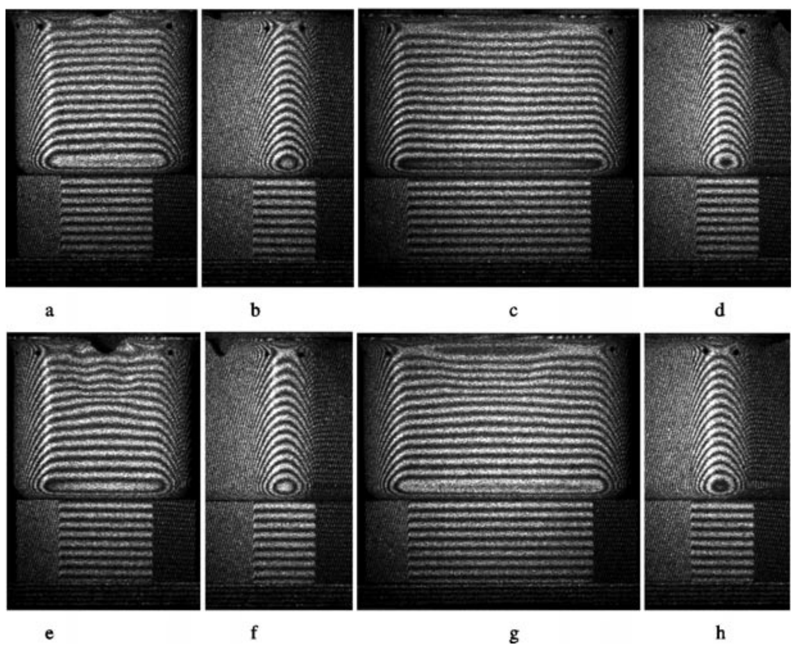

Figure 9. Single acquired modulated fringe patterns.

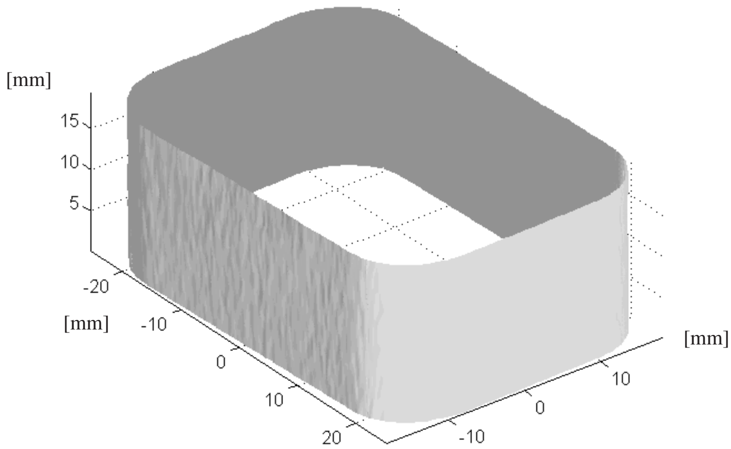

Figure 10. Rebuilt total lateral surface of the specimen.

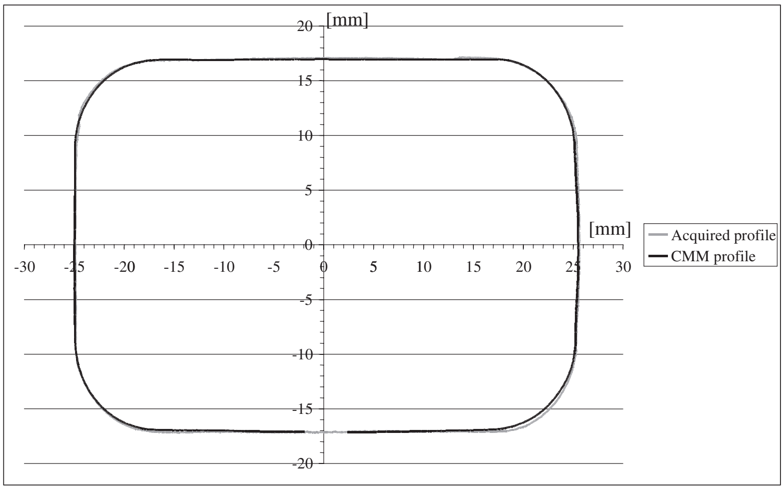

Figure 11. CMM and proposed technique results at $z = 17.5$ mm.

figures 9(*a*)–(*h*). In figure 10 the final rebuilding of the lateral surface of the specimen is shown.

Finally the obtained results were compared with measurements done at the Department of Mechanics and Management Engineering (Padua University, Italy) by CMM Zeiss Prismo Vast 7 HTG. In particular in figure 11 the comparison between the obtained profile and the measurements provided by the contact technique is reported for a horizontal measurement section at $z = 17.5$ mm from the bottom internal surface of the specimen. A global very good overlapping is observed. However, a closer examination shows slight discrepancies near the corners of the specimen. Such mismatching is mainly due to the utilized rebuilding procedure. The same comparison was repeated for each single basic surface and a satisfying agreement was obtained. In particular, figure 12 reports a quantitative numerical comparison between the results obtained with the proposed system and the CMM ones taken along one horizontal profile ($z = 17.5$ mm) belonging to the front long edge (figure 9(*g*)). This result is consistent with the evaluated uncertainty; it confirms the effectiveness of the method to measure and digitize with the required accuracy flat surfaces characterized by small shape errors.

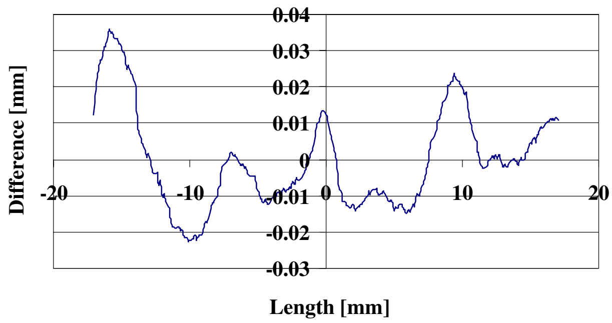

Figure 12. Quantitative numerical comparison between the obtained and the CMM results (image 9g).

7. Conclusions

In this paper, an optical technique to measure and digitize 3D surfaces has been developed. The technique, moving from a typical shadow moiré set-up, implements a few variations in order to introduce a carrier fringe pattern to significantly improve spatial resolution, overcoming some inherent shortcomings in the conventional method. The proposed technique appears simpler than others found in the literature.

Such characteristics enable the developed technique to be very suitable for the measurement of stamped parts, usually characterized by large flat areas, assuring proper resolution and low level of uncertainty. In this way it could be utilized in different fields such as reverse engineering applications and shape defect detection. Furthermore, its non-contact nature guarantees the absence of any interaction (instrument–measurand) which could alter the measurand itself.

Moreover, a specific image processing software was developed in order to obtain measurement data from each of the acquired fringe pattern fields. A proper rebuilding procedure was then set up with the aim to merge the single digitized surfaces into the whole lateral surface of the investigated specimen.

The obtained results were compared with measurement results given by a CMM, showing an appreciable agreement.

The proposed technique appears to be promising for measurement and digitization of soft material components.

Acknowledgments

This work has been made possible by funds from MURST (Italian Ministry of the University and Scientific Research). The authors are grateful to the Department of Mechanics and Management Engineering of Padua University (Italy) for the measurements done by Zeiss Prismo Vast 7 HTG.

Appendix

To ensure an effective filtering operation, the following inequalities must be satisfied

$$\begin{aligned} \omega_{1M} &< \omega_{nm} \\ \omega_b &< \omega_{1m}. \end{aligned} \tag{A.1}$$

This in turn can be expressed as

$$\omega_c + \left.\frac{\partial\varphi}{\partial x}\right|_M < n\left(\omega_c + \left.\frac{\partial\varphi}{\partial x}\right|_m\right) \qquad n = 2, 3, \ldots,$$

$$\omega_b < \omega_c + \left.\frac{\partial\varphi}{\partial x}\right|_m.$$

A more severe condition is represented by the inequalities

$$\begin{aligned} \omega_c + \left.\frac{\partial\varphi}{\partial x}\right|_M &< n\left(\omega_c - \left.\frac{\partial\varphi}{\partial x}\right|_m\right) \qquad n = 2, 3, \ldots, \\ \omega_b &< \omega_c - \left.\frac{\partial\varphi}{\partial x}\right|_m \end{aligned} \tag{A.2}$$

and after a few simple mathematical steps the conditions can be formalized as

$$\begin{aligned} \left.\frac{\partial\varphi}{\partial x}\right|_M &< \omega_c\left(\frac{n-1}{n+1}\right) \\ \left.\frac{\partial\varphi}{\partial x}\right|_M &< \frac{\omega_c}{2} \end{aligned} \tag{A.3}$$

with the assumption $\omega_b \ll \omega_c$. In expression (A.3) $(\partial\varphi/\partial x)|_M$ has been substituted to $(\partial\varphi/\partial x)|_m$.

Since the ratio $(n-1)/(n+1)$ monotonically increases with n, as

$$\lim_{n\to+\infty} \frac{n-1}{n+1} = 1 \tag{A.4}$$

with a minimum (non-zero) value (1/3) at $n = 2$, the previous set of inequalities in expression (A.3), are rewritten as

$$\left.\begin{aligned} \left.\frac{\partial\varphi}{\partial x}\right|_M &< \frac{\omega_c}{3} \\ \left.\frac{\partial\varphi}{\partial x}\right|_M &< \frac{\omega_c}{2} \end{aligned}\right. \Rightarrow \quad \left.\frac{\partial\varphi}{\partial x}\right|_M < \frac{\omega_c}{3}. \tag{A.5}$$

Moving from the expression in equation (23)

$$h = \frac{p\varphi}{2\pi(\tan\alpha + \tan\beta)} = \frac{p\varphi L}{2\pi D} \tag{A.6}$$

the expression of $\varphi(x)$ becomes

$$\varphi = \varphi(x) = 2\pi\frac{D}{pL}h(x). \tag{A.7}$$

Introducing the conditions formulated in equation (A.5), it follows that

$$\begin{gathered} \left.\frac{\partial\varphi}{\partial x}\right|_M = 2\pi\frac{D}{pL}\left.\frac{\partial h}{\partial x}\right|_M < \frac{\omega_c}{3} \\ \left.\frac{\partial h}{\partial x}\right|_M < \frac{2\pi f_c}{3}\frac{Lp}{D}\frac{1}{2\pi} = \frac{1}{3}f_c\frac{Lp}{D} \Rightarrow \left.\frac{\partial h}{\partial x}\right|_M < \frac{1}{3}f_c\frac{Lp}{D} \end{gathered} \tag{A.8}$$

where $f_c = \omega_c/2\pi$.

The condition to be satisfied for a correct application of the FT method to the measured signal of interest has been obtained. It ensures the effective separation between the signal bandwidth carrying the information about the phase distribution along the measured surface and both the low-frequency bandwidth components (intensity bias) and the high-frequency bandwidth ones (unwanted high-frequency noise) which carry no information concerning the surface under investigation. Therefore, once the value of the parameter $\left.\frac{\partial h}{\partial x}\right|_M$ is known, the experimental set-up parameters (L, D, p and f_c) must be chosen accordingly, in order to guarantee that the condition expressed in equation (A.8) is satisfied.

Within certain limits, this condition can be satisfied by simply increasing the grid slope, with no experimental complication of the set-up. This confirms the adaptability of the proposed technique.

References

[1] Chen F, Brown G M and Song M 2000 Overview of three-dimensional shape measurement using optical methods *Opt. Eng.* **39** 10–22

[2] Kobayashi A 1991 New optical measurements and their applications in industry *Measurement* **9** 88–96

[3] Osawa S, Furutani R, Takamasu K, Shigeo O and Asano H 1999 3D shape measurement by self-referenced pattern projection method *Measurement* **26** 157–66

[4] Post D, Han B and Ifjiu P 1994 *High Sensitivity Moiré* (New York: Springer) pp 119–24, pp 419–26

[5] Patorski K 1993 *Handbook of The Moiré Fringe Technique* (New York: Elsevier) pp 220–49, pp 254–322
[6] Cloud G 1995 *Optical Methods of Engineering Analysis* (Cambridge: Cambridge University Press)
[7] Wang M 1996 Projection moiré deflectometry for the automatic measurement of phase objects *Opt. Eng.* **35** 2005–11
[8] Cline H E, Lorensen W E and Holik A S 1984 Automatic moiré contouring *Appl. Opt.* **23** 1454–9
[9] Halioua M, Krisnamurty R S, Liu H and Chiang F P 1983 Projection moiré with moving gratings for automated 3D topography *Appl. Opt.* **22** 850–5
[10] Matsumoto T, Kitagawa Y and Minemoto T 1996 Sensitivity-variable moiré topography with a phase shift method *Opt. Eng.* **35** 1754–60
[11] Czarnek R and Guo Y 1991 Surface contouring using virtual gratings *Exp. Tech.* 35–7
[12] Takeda M, Ina H and Kobayashi S 1982 Fourier transform method of fringe pattern analysis for computer based topography and interferometry *J. Opt. Soc. Am.* **72** 156–60
[13] Wang B, Luo X, Pfeifer T and Mischo H 1999 Moiré deflectometry based on Fourier-transform analysis *Measurement* **25** 249–53
[14] Takeda M and Mutoh K 1983 Fourier transform profilometry for the automatic measurement of 3-D object shapes *Appl. Opt.* **22** 3977–82
[15] Zwemer D, Hassell P, Mazeika W, Petersek L and Holmes R 1997 Shadow moiré based printed wiring board flatness inspection *Proc. Technical Conf. on IP Printed Circuits EXPO (San Jose CA, USA, March 1997)* p 802 webpage http://www.warpfinder.com/IPC.pdf
[16] Wang Y and Hassell P 1997 Measurement of thermal deformation of BGA using phase-shifting shadow moiré *Post Conf. Proc., SEM 97 Spring Conf. (Bellevue, WA)*
[17] Zhang X and North W P T 1998 Phase shifting method for retroreflective grating analysis *Strain* November 123–6
[18] Nigrelli V and Petrucci G 1991 Il rilievo e la rappresentazione di superfici con la tecnica del Moiré ombra *VII Convegno ADM (Trento, Italy, September 1991)* pp 103–15
[19] Yoshizawa T and Tomisawa T 1993 Shadow moiré topography by means of the phase shifting method *Opt. Eng.* **32** 1668–74
[20] Jin L, Kodera Y, Yoshizawa T and Otani Y 2000 Shadow moiré profilometry using the phase shifting method *Opt. Eng.* **39** 2119–23
[21] Xie X, Lalor N J, Burton D R and Shaw M N 1997 Four-map absolute distance contouring *Opt. Eng.* **36** 2517–20
[22] Jin L, Otani Y and Yoshizawa T 2001 Shadow moiré profilometry by frequency sweeping *Opt. Eng.* **40** 1383–6
[23] Mauvoisin G, Bremand F and Lagarde A 1994 Three-dimensional shape reconstruction by phase shifting shadow moiré *Appl. Opt.* **33** 2163–9
[24] Green R J, Walker J G and Robinson D W 1988 Investigation of the Fourier-transform method of fringe pattern analysis *Opt. Lasers Eng.* **8** 29–44
[25] Kreis T 1986 Digital holographic interference-phase measurement using Fourier transform method *J. Opt. Soc. Am.* A **3** 847–55
[26] Sciammarella C A and Ahnadshahi M A 1986 Detection of fringe pattern information using a computer based method *Proc. 8th Int. Conf. on Experimental Stress Analysis* pp 359–68
[27] Sciammarella C A and Bhat G 1992 Two-dimensional Fourier transform methods for fringe pattern analysis *Proc. 7th Int. Conf. on Experimental Mechanics (Las Vegas, USA)*
[28] Sciammarella C A and Sturgeon D L 1967 Digital filtering techniques applied to the interpolation of moiré-fringe data *Exp. Mech.* **7** 468–75
[29] Petrucci G 1999 Alcuni aspetti teorici e pratici del metodo della trasformata di Fourier in fotomeccanica *28th Convegno Nazionale AIAS (Vicenza, Italy, September 1999)* pp 797–806
[30] ISO 1993 *Guide to the Expression of Uncertainty in Measurement* (Geneva: ISO)
[31] Heipke C 1992 A global approach for least-squares image matching and surface reconstruction object space *Photogramm. Eng. Remote Sens.* **58** 317–23